Cellulose (2021) 28:2215–2228
https://doi.org/10.1007/s10570-020-03656-y

ORIGINAL RESEARCH

Solvothermal sol–gel synthesis of TiO_2-cellulose nanocrystalline composites

Andrey Zdravkov · Maria Listratenko · Stanislav Gorbachev · Iraida Osovskaya · Andrey Kanaev · Nikolai Khimich

Received: 13 August 2020 / Accepted: 17 December 2020 / Published online: 15 January 2021
© The Author(s), under exclusive licence to Springer Nature B.V. part of Springer Nature 2021

Abstract Due to its unique supramolecular structure, cellulose is widely used as a template agent, ensuring an easy structuring of anatase TiO_2 particles with subsequent release after the organics burning. This work is devoted to the synthesis of microcrystalline cellulose-TiO_2 (MCC-TiO_2) composite photocatalyst by preserving the intermediate organic–inorganic structures. A series of the MCC-TiO_2 materials were prepared via solvothermal sol–gel method in n-decane and caproic acid solvents and characterized by X-ray diffraction, transmission electron microscopy, IR spectroscopy, ^{1}H NMR and TG/DSC methods. The photocatalytic activity of the prepared materials was evaluated by the decomposition of formic acid in aqueous solutions. The composites failed to be formed in n-decane, while in caproic acid, acting as solvent and reagent, anatase TiO_2 nanoparticles were formed onto the crystalline domains of cellulose, tightly fixed due to covalent Ti–O–C bonds. The materials formed in caproic acid showed a higher photocatalytic activity, explained by a complementarity of the organic and inorganic components. The specific activity (normalized on TiO_2 mass) of best synthetized composite materials was almost twice higher than that of Aeroxide P25 TiO_2 reference photocatalyst.

Supplementary Information The online version contains supplementary material available at (https://doi.org/10.1007/s10570-020-03656-y).

A. Zdravkov
Grebenshchikov Institute of Silicate Chemistry, Russian Academy of Sciences, Makarova emb. 2, 199034 St. Petersburg, Russian Federation

M. Listratenko · N. Khimich (✉)
Kirov Military Medical Academy, Academika Lebedeva str. 6, 194044 St. Petersburg, Russian Federation
e-mail: n.n.khimich@gmail.com

S. Gorbachev · I. Osovskaya
St. Petersburg State University of Industrial Technology and Design the Higher School of Technologies and Power Engineering, Ivana Chernykh str. 4, 198095 St. Petersburg, Russian Federation

A. Kanaev
Laboratoire Des Science Des Procédés Et Des Matériaux, CNRS, Université Sorbonne Paris Nord, 93430 Villetaneuse, France

Graphic abstract

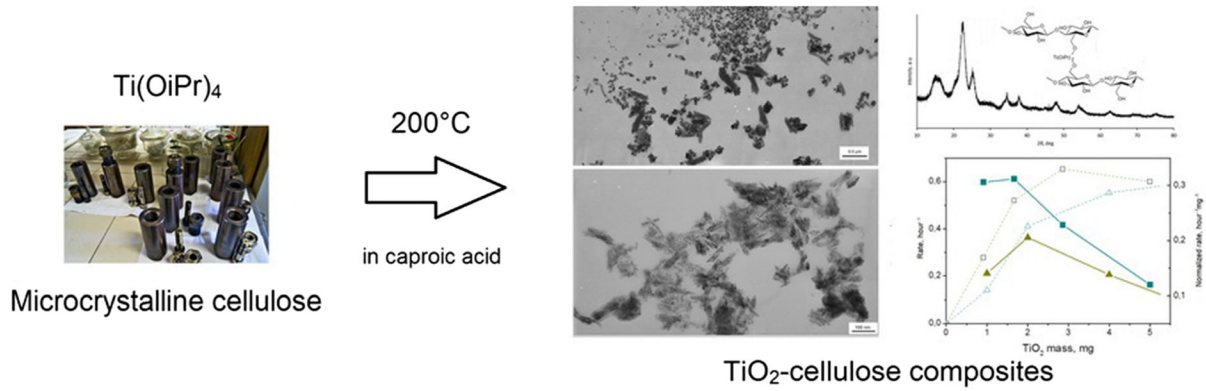

Keywords Microcrystalline cellulose-titania composite · Solvothermal synthesis · Sol–gel

Introduction

Among different semiconductors (TiO_2, WO_3, Fe_2O_3, $SrTiO_3$, ZnO, etc.) that can be used in photocatalytic process for degradation of organic pollutants, TiO_2 has received a particular interest because of its high activity, chemical stability, relatively low cost and low toxicity (Mory 2005; Sharon et al. 2016; Tang et al. 2018). However, the research on the improved photocatalyst design is still under way. Between different approaches, composite materials can be an interesting solution capable affecting charge separation and trapping effectiveness and light absorption efficiency. A striking example of a two-component system of noble metal and semiconductor particles can be given (Zhang et al. 2013), which synergy is based on a Schottky junction and localized surface plasmon resonance. Excellent charge separation efficiency can also take place in composite or hybrid species including inorganic TiO_2 and organic polymer components (Kuznetsov et al. 2009; Gorbovyi et al. 2011). The synthesis of such materials has overcome numerous problems, related to the preparation of ensembles of freestanding particles, their uniform distribution free of aggregation, and link to the host polymer by strong covalent bonds.

Both inorganic [e.g. montmorillonite (Tieng et al. 2011)] and organic [e.g. polyamide-amine-epichlorohydrin (Wang et al. 2015), polylactide (Kaseem et al. 2019)] polymers can be taken as complementary components of photocatalytic materials. At the same time, use of natural biopolymer cellulose could be a particularly attractive solution (Dette et al. 2014; Filippo et al. 2015; Sathasivam et al. 2015; He et al. 2016; Butman et al. 2018; Garusinghe et al. 2018; Rahmawati et al. 2017; Wittmar et al. 2015; Oliveira et al. 2017; Shahrezaei et al. 2017.; Melvin et al. 2019; Habibi et al. 2020). Cellulose does not absorb in the UV–visible spectral range (Sirvio et al. 2016) and cannot screen action spectrum of the photoactive TiO_2 component. A very interesting supramolecular structure and multilevel structural organization of this polymer (Farag et al. 2017) explains its wide use as a template agent (Ioelovich 2014; Lu et al. 2013; Wang et al. 2016; Kayaalp et al. 2014; Xiao et al. 2017; Postnova et al. 2015; Zlotski and Uglov 2017; Shevtsova and Zlotski 2018; Brandes et al. 2016), ensuring an easy structuring of anatase TiO_2 particles. The thermal post-treatment performed in the related studies has resulted in a burnout of the organic component with subsequent formation of anatase nanoparticles with the shape and size control, exhibiting photocatalytic activity (Postnova et al. 2015). Naturally, cellulose degrades in these conditions leading to the decomposition of the intermediate structures. Attempts to preserve the organic component in the final photocatalyst are rare (Galkina et al. 2014; Khalid et al. 2017; Luo et al. 2014; Morawski et al. 2013; Melvin et al. 2019; Sun et al. 2010). The synthesis by decomposition of titanium isopropoxide in ethanol media together with wood cellulose fibers in the microwave-assisted solvothermal process has been reported by Cardoso et al. (2018) and the mechanism

of the nucleation and growth of TiO_2 nanoparticles on cellulose fibers has been depicted. Although photocatalytic applications were suggested, no evaluation of the material activity has been presented in this study. The photocatalyst preparation via low-temperature sol–gel method has been reported by Morshed et al. (2020) and its activity on methylene blue dye decomposition in aqueous solution (pH = 6) under UV light resulted in the first order kinetics with rate constant of 0.188 1/min. The material has shown a good stability with negligible deactivation after 5 recycling. Very recently, Li et al. (2020) have realized a controlled synthesis of TiO_2-cellulose nanocomposites via biotemplate method and assigned an enhanced photocatalytic activity to the ligand-to-metal charge transfer complex at the interface between the components. In this study, the material activity has been evaluated on Cr(VI) reduction in particular acid conditions at pH = 3 in the visible spectral range of $\lambda \geq 420$ nm and compared with P25 TiO_2, which is a well-known UV-sensible reference photocatalyst offering a weak absorbance in acid media. Because of this, this activity concerned participation of intraband defect levels and not to the common photocatalytic mechanism involving the interband electronic transitions. Many points, including the component mass ratio and type of binding between the constituting organic and inorganic components have to be explored in order to understand potentiality of the TiO_2-cellulose nanocomposites in photocatalysis.

In this work, we developed a method for synthesis of a composite material, consisting of TiO_2 nanoparticles strongly bound to microcrystalline cellulose and possessing an enhanced photocatalytic activity owing to a specific participation of both constituting components.

Experimental

Caproic acid (Aldrich, 98%), n-decane (Aldrich, 99%), titanium tetraisopropoxide (TTIP, Aldrich, 97%) and microcrystalline cellulose (MCC, Aldrich, 10 wt. % H_2O) were used in the synthesis. Caproic acid and n-decane were additionally dried over molecular sieves (Merck). To obtain anhydrous cellulose if necessary, the commercial MCC was dried at 110 °C in a vacuum (0.1 mm Hg). All manipulations preceding the heat treatment in an autoclave were performed in a glove box filled with dry argon.

In a typical experiment, TTIP was dissolved in 15 mL of caproic acid (or in 15 mL of n-decane), and 1 g of MCC was added. After a thorough mixing, the reaction mixture was placed in a Teflon liner of a steel autoclave (internal volume 50 mL) under argon and heated to 200 °C. The samples were separated on a Schott filter, washed successively with decane, petroleum ether, and alcohol and dried thereafter without any contact with atmospheric moisture.

The samples were examined by IR spectroscopy (FSM-2201 device) and X-ray diffraction (Rigaku SmartLab 3 diffractometer, CuK_α radiation, $\lambda = 1.54051$ Å) methods. The particle crystalline size was determined from the (101) diffraction line width using the Scherrer equation. The crystallinity index (CrI) was calculated as the ratio of the highest peak (crystalline peak I_{200}) to that of the minimum (I_{am}) (Segal et al. 1959) between the (110) and (102)/(012) peaks at about $2\theta = 18.5°$ (French 2014). Examination of each of the sample (MCC, TiC(1–4)) results in curves whose measured heights above a base line at $2\theta = 18.5°$ and 22.8° gave the value I_{am} and I_{200} respectively.

$$\mathrm{CrI} = \frac{I_{200} - I_{am}}{I_{200}}$$

The specific surface area was estimated by the BET method, pore volume, and average pore size were estimated by the BJH method from the nitrogen adsorption/desorption isotherms measured with Quantachrome NOVA 1200e instrument. For measurements samples were treated at 110 °C in vacuum (< 0.1 mmHg) for 2 h. The transmission electron micrographs (TEM) were taken with a JEOL JEM-100C device, after preparing the analytic samples in chloroform. ^{1}H NMR spectra were recorded with JEOL ECX-400A instrument at 400 MHz, after preparing the analytic samples in benzene-d_6. The UV–visible absorption spectra of the samples prepared were measured with SF-2000 spectrometer equipped with an integrating sphere. The thermal analysis was performed with Netzsch STA 429 device under dry argon gas atmosphere.

The photocatalytic activity of the materials prepared was evaluated by monitoring the decomposition of formic acid ($pK_a = 3.75$, initial concentration 0.35 mmol/l) in aqueous solution of a total volume

100 mL. Prior to UVA irradiation, every synthetized sample of 10 mg mass was dispersed during 10 min under ultrasound in 1 mL of water until a stable suspension of was formed. When using caproic acid, 1% KOH solution was taken instead of water, with the subsequent neutralization to pH 5. The photocatalytic medium was prepared under air flow in a dark under magnetic stirring for 30 min. The prepared suspensions were irradiated with a DRL-100 high-pressure mercury lamp under continuous magnetic stirring. The lamp emits in the UV–visible range with the most intense UVA line at $\sim$ 365 nm (90% of the lamp intensity). The reaction solutions were periodically analyzed, and the initial (C_0, t = 0) and current (C, t > 0) formic acid concentrations were calculated from the solution acidity. The solution acidity was

Table 1 Synthesis conditions and photocatalytic rate constant (R) of TiO_2–MCC composites

Sample	Solvent	Reaction time (h)	TiO_2 content (g)**	R (h^{-1})***	Error bars +/−
$TiDH_2O$	n-decane	8	0.27	0.100	0.005
TiD1	n-decane	8	0.27	0.153	0.006
TiD2	n-decane	15	0.27	0.195	0.008
TiD3	n-decane	30	0.27	0.223	0.008
TiO_2D2*	n-decane	15	0.27	0.273	0.017
TiC1	Caproic acid	8	0.05	0.278	0.011
TiC2	Caproic acid	8	0.13	0.520	0.020
TiC3	Caproic acid	8	0.27	0.600	0.033
TiC4	Caproic acid	8	0.54	0.654	0.036
TiC5	Caproic acid	2	0.27	0.408	0.011
TiC6	Caproic acid	4	0.27	0.458	0.012
TiO_2C3*	Caproic acid	8	0.27	0.343	0.010
TiO_2 P25				0.732	0.040

*Samples prepared with an additional calcination at 500 °C for 2 h

**TiO_2 content corresponds to the initial TTIP amount mixed with 1 g MCC

***Corresponds to the first order kinetics. Tests were performed with 10 mg powders

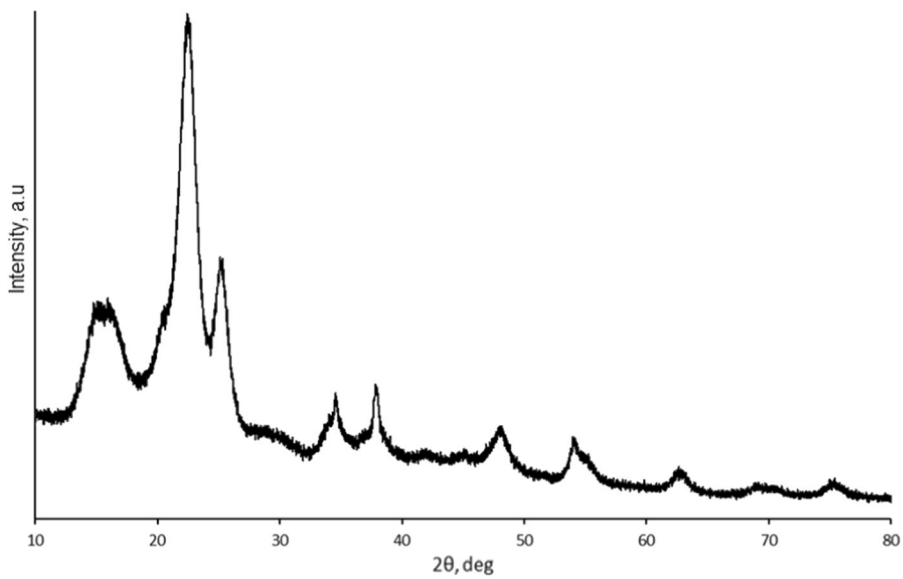

Fig. 1 X-ray diffraction data of $TiDH_2O$ sample

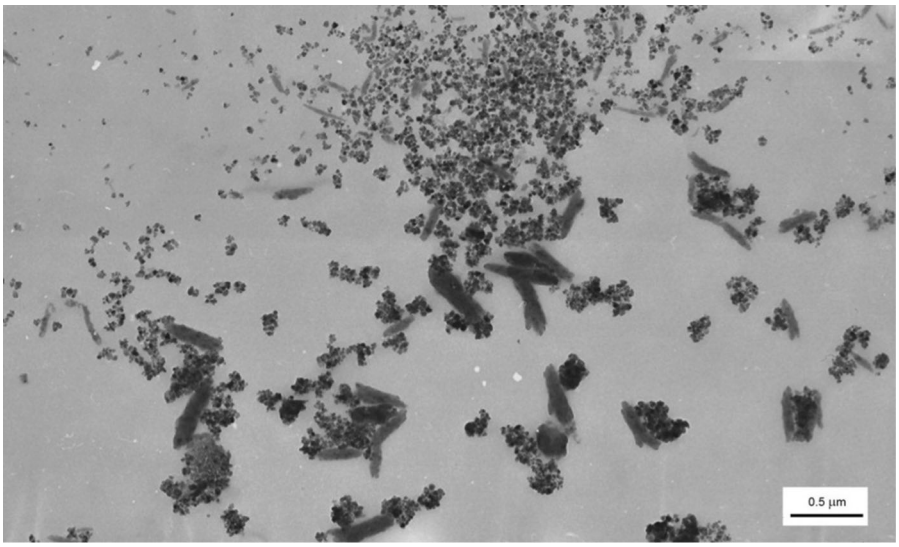

Fig. 2 TEM micrograph of $TiDH_2O$ sample

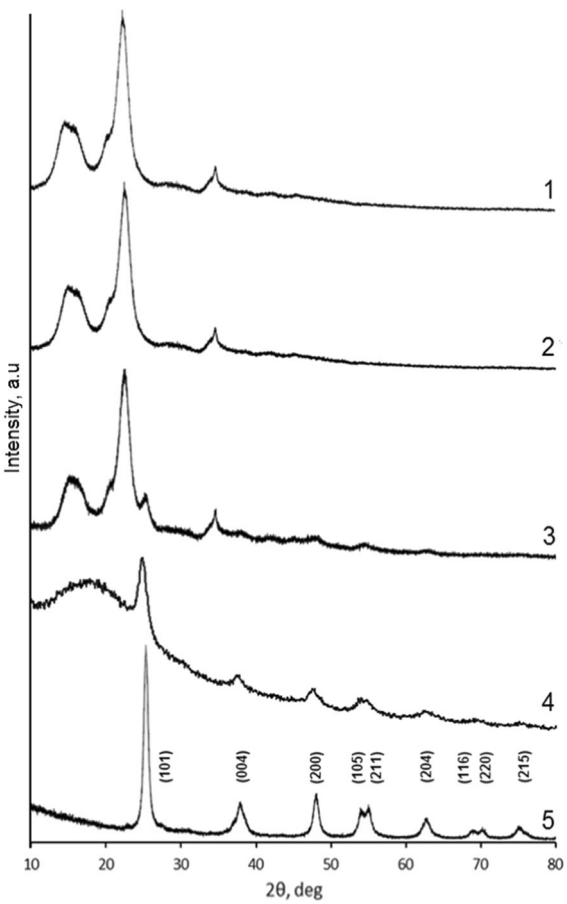

Fig. 3 X-ray diffraction data of MCC (1), TiD1 (2), TiD2 (3), TiD3 (4) and TiO_2D2 (5)

determined with an I-510 ionometric converter with an accuracy of ± 0.01 pH unit. Aeroxide P25 TiO_2 (Sigma-Aldrich) of a mean particle size 21 nm and specific surface area 35–65 m^2/g (BET) was used as a reference sample.

To evaluate the effect of the mass exchange on the rate of photocatalytic decomposition of formic acid, the stirring rate of the photocatalytic medium was varied from 200 to 800 rpm. These measurements revealed no appreciable influence of stirring on the decomposition rate, which permits to conclude that the mass transport was not a limiting stage in our experimental conditions and that the decomposition rate depends mostly on the material activity.

A list of the synthesized samples along with their preparation conditions are summarized in Table 1. Samples indicated as TiD and TiC were respectively prepared in decane and in caproic acid and samples $TiDH_2O$ and TiO_2D_2 were prepared in decane from commercial cellulose. The synthesis of all samples was performed at 200 °C. The details of preparation given in Table 1.

Results and discussion

Our attempts failed to prepare anatase TiO_2-MCC composites using the commercial MCC. This is apparently due to the fact that hygroscopic cellulose contains about 10 wt% of water. The X-ray diffraction

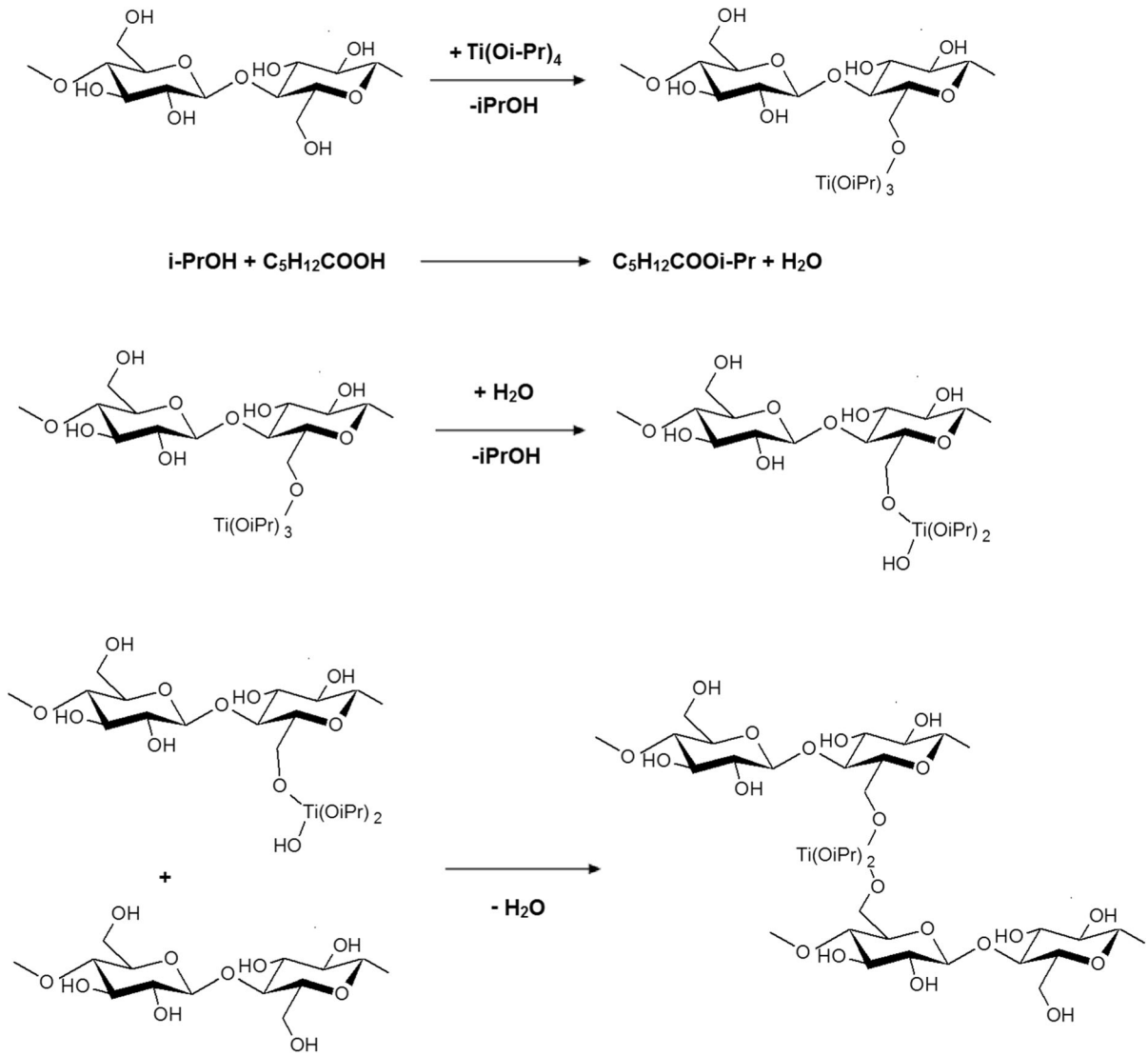

Fig. 4 Tentative reaction scheme

analysis of $TiDH_2O$ sample (Fig. 1) showed that nanosized anatase is formed when performing the synthesis in TTIP–MCC (commercial)–*n*-decane system but anatase and MCC behave as the independent components. In fact, TEM micrograph in Fig. 2 clearly shows that majority of anatase TiO_2 crystallites were separated from MCC grains, forming a mixture of a priory non-interacting particles ($TiDH_2O$). An increase in the cellulose grain size may be attributed to a partial grains sintering. In this case, one cannot expect any synergy revealed by the material components in the photocatalytic process.

The reaction of TTIP with anhydrous MCC in n-decane is rather slow, as confirmed by the fact that Bragg reflections of anatase TiO_2 did not significantly show up in X-ray diffraction pattern of TiD1 sample (Fig. 3), even after 8 h of the reaction runtime, which pattern is almost identical to that of pure cellulose (MCC).

The titania attachment to the cellulose surface begins in these conditions through the condensation reactions between the most active hydroxy group of cellulose at C^6 carbon atom and OR- of Ti cation with the release of isopropyl alcohol (Fig. 4).

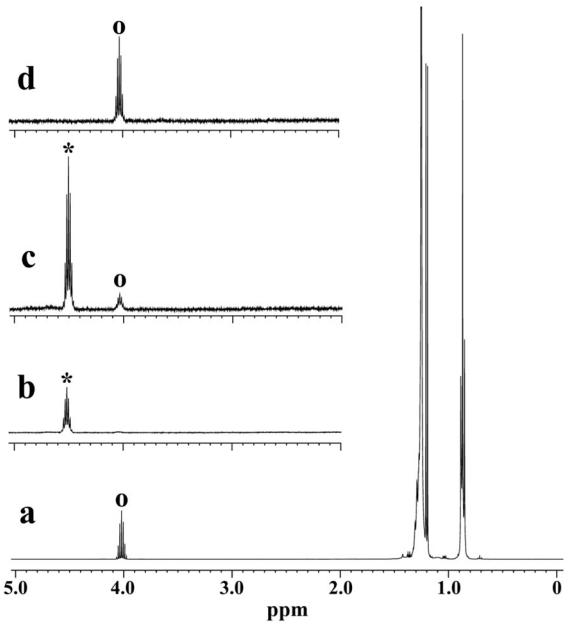

Fig. 5. ^{1}H NMR spectra of isopropyl alcohol in decane (**a**), TTIP in decane (**b**), reaction mixture after 2 h (**c**), reaction mixture after 8 h (**d**)

This process was confirmed by ^{1}H NMR measurements shown in Fig. 5. Two solutions of TTIP and isopropyl alcohol in decane and reference samples were examined in this series. The signal of the decane proton was observed in all spectra at high fields ($\delta < 1.5$ m.d). The proton of the secondary carbon atom in TTIP gives a septet at 4.50 ppm (J = 6.18 Hz), and the relevant proton in isopropyl alcohol molecule gives a septet at 4.03 ppm (J = 6.11). The solvothermal process leads to smearing of the septet, suggesting distortion symmetry of the substituents at the titanium atom when isopropyl alcohol appears. We notice that the control series performed without TTIP showed that MCC was stable in the experimental conditions with the weight loss of the material below 0.2% during 8 h of the autoclave treatment. A noticeable amount of anatase TiO_2 was only obtained after a heat treatment of the reaction mixture in the autoclave for a longer time (TiD2 and TiD3 samples) and/or higher temperature (TiO_2D_2 sample), as show X-ray diffraction patterns of in Fig. 3. However, cellulose underwent a gradual degradation in this case; this can be seen from comparison of curves 2, 3 and 4, where reflexes of MCC continuously weakened and disappeared.

In order to obtain a stable anatase TiO_2-MCC composite, n-decane solvent, which did not work, was replaced by caproic acid contributed to the synthesis as reagent and solvent in the same time. In the caproic acid medium, water is released in situ, and this fact allows the composite formation process to be controlled. This mechanism has been previously studied in Zdravkov et al. (2015). Figure 6 shows that the formation of the anatase structure occurs already in the first 2 h of the reaction and the formation of anatase TiO_2-MCC composite was completed after 8 h.

According to TEM images in Fig. 7, the synthesis is accompanied by loosening of MCC grains in course of the anatase immobilization. This process is accompanied by a partial cellulose degradation, which was confirmed by nitrogen sorption/desorption data. The surface area, pore volume, and pore diameter of TiC samples with different titania contents and those of the reference Aeroxide P25 TiO_2 are summarized in Table 2. These parameters suggest high adsorption activity of samples TiC1, TiC3, and, especially, TiC4. The isotherms evaluated for MCC-TiO_2 composites were classed with type IV and V isotherms, suggesting the micro- and mesoporous character of the samples. For sample TiC4, the amount of nitrogen adsorbed rapidly increases at all relative pressures, reaching 95 cm^3/g (Fig. 8d). The pore size distribution for sample TiC4 has a single narrow peak indicating that this sample is highly homogeneous.

Isotherms and pore radius distributions for samples TiC1 and TiC3 have the similar shape, but the amount of adsorbed nitrogen is different (for TiC1, the amount is 20 cm^3/g (Fig. 8b), and for TiC3, the amount is 40 cm^3/g (Fig. 8c)). For initial MCC the amount of nitrogen adsorbed is comparatively low—near 3 cm^3/g, and pore size distribution was wide with several different predominant pore sizes (see Figure S8. Supporting Information). As one can see in the course of synthesis the pore size distribution became narrow. It supported the assumption, that reaction of cellulose and titanium isopropoxide goes especially at amorphous regions.

The specific surface area of TC samples proportionally increases with the increase of titania content, which is characteristic of particles undergoing insignificant coarsening. The mean size of TC series crystalline particles, calculated by Scherrer equation from curves 3 and 4 (Fig. 3) and curve 3 (Fig. 6) was about 30 nm.

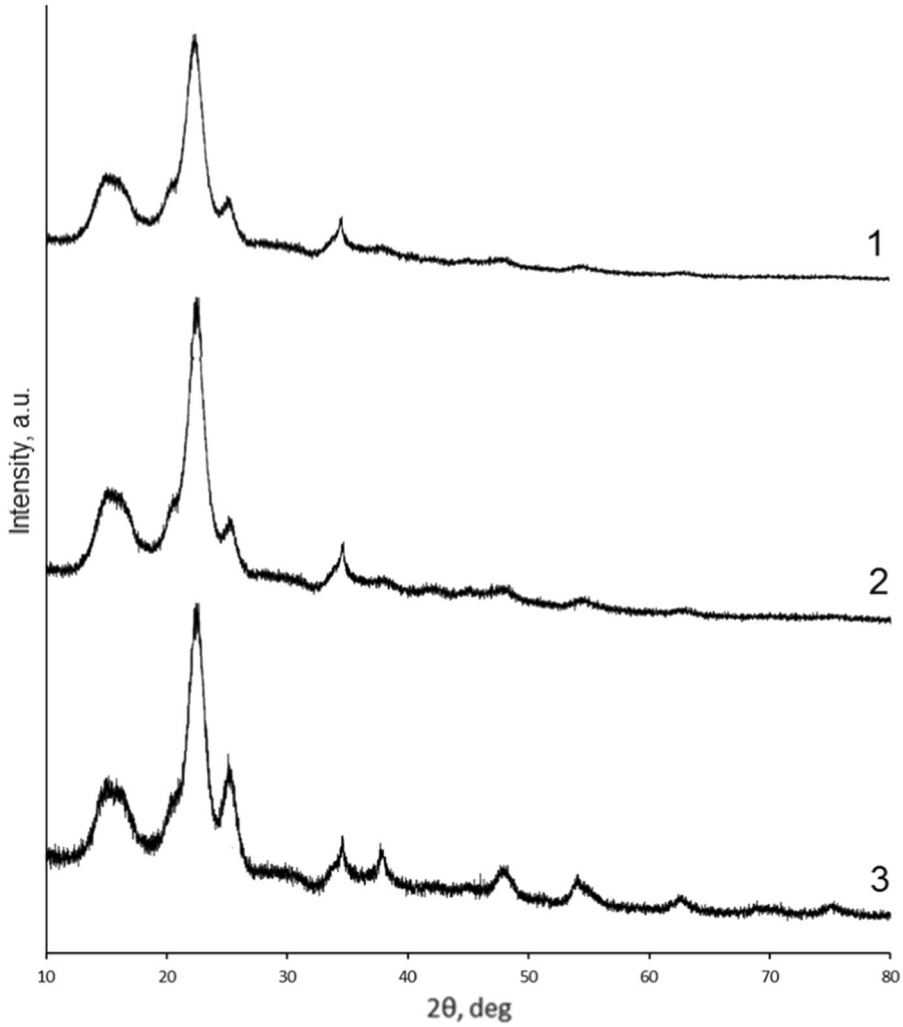

Fig. 6 X-ray diffraction data of TiC5 (1), TiC6 (2), TiC3 (3)

At the same time, during the formation of MCC-TiO_2 composite, the degree of crystallinity of cellulose increases from 91% (pure MCC) to 98% (TiC4) with an increase in the concentration of titanium dioxide. This can be explained by the fact that the reaction between the components (Eqs. 1–4) proceeds primarily through the most accessible and active groups located in the amorphous regions. The data on crystallinity of cellulose were obtained by Segal method (Segal et al. 1959; Yacenko et al. 2019). For more details, see Supporting Information.

The formation of anatase TiO_2-MCCcomposites was also confirmed by FTIR spectroscopy and thermal analysis. An example of pure cellulose MCC and composite TiC4 sample with the highest titania content (see Table 1) is given in Fig. 9. The strong IR band of hydroxyl bending vibrations in cellulose at 1630 cm^{-1} was observed to shift to lower frequencies upon the composite formation, down to 1620 cm^{-1} in TiC4, suggesting strong interfacial interaction between hydroxy groups of MCC and cations of titania nanoparticles. In the case of TiD sample this shift in IR spectrum was not observed. The same conclusion can be drawn from the shift of the stretching vibration band of cellulose hydroxyls at 3430 cm^{-1} to lower frequencies: 3410 cm^{-1} in the composite material (Fig. 9). The TG-DSC analysis indicated a progressive decomposition of cellulose with an increase of temperature, accompanied by a release of different gaseous products including

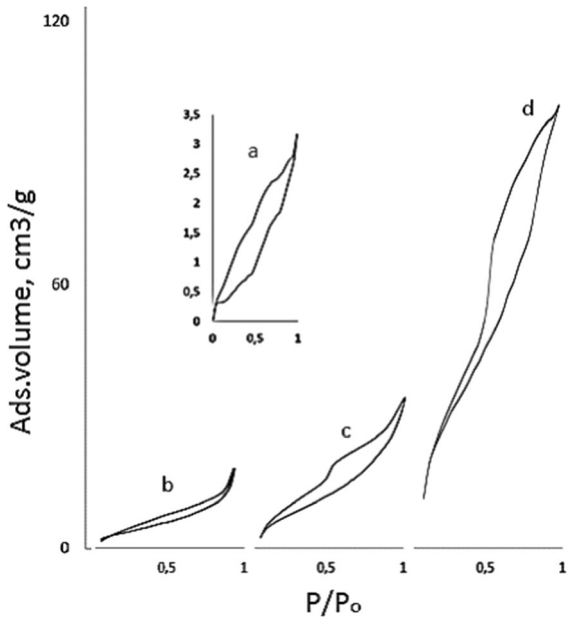

Fig. 7 TEM micrographs of MCC (**a**) and TiC4 (**b**) samples

hydrogen, methane, carbon monoxide, etc. The thermolysis process in argon atmosphere is characterized by endothermic peaks of DSC curves. The results in Fig. 10 show that the main endothermic peak of MCC was shifted to higher temperatures by 42 °C in TiC4 composite while its magnitude was decreased from 1.32 to 0.57 mW/mg. This confirms a tight coupling between the two components of the composite. The ~ 50% weight loss in the temperature range of thermolysis, observed in TiC4 compared with MCC, validates the presence of stable inorganics.

In the photocatalytic experiments, formic acid was used as a model pollutant not sensitive to UVA radiation, which favorably distinguishes it from commonly used dyes rhodamine and methylene blue. The kinetics of the formic acid degradation is shown in Figs. 11 and 12 in a semi-logarithmic frame, which evidences the first order decomposition kinetics, far from saturation phenomena. The photocatalytic rate constants in Table 1 were obtained from the linear least-squared fits of the experimental date. The kinetics observed with TD samples was relatively slow (Fig. 13). The thermal post-treatment (TiO_2D sample) did not significantly enhance the material activity, which remained much slower compared to that of commercial TiO_2 P25 photocatalysts. This correlates with our XRD measurements shown poor crystallization of anatase TiO_2 in the n-decane synthesis conditions. In contrast, TC samples synthesized in caproic acid exhibited an appreciably faster kinetics (Fig. 11) corresponding to their higher photocatalytic activity; among these samples, TiC4 prepared with the highest titania content possessed the highest activity. We notice that because of a steric factor, the hydroxy group at C-6 carbon atom of cellulose is expected to be most active in the titania attraction. Because of this, the effective amount of anatase in the composite material cannot exceed a limit imposed by the cellulose content, which is expected to be about 50 wt%. Apparently, this limit is attaint in TiC4 sample and further increase of the titania content is inappropriate.

A deeper comparison between our best prepared and reference TiO_2 P25 photocatalysts can be performed based on the intrinsic efficiency γ defined as the conversion yield of an absorbed photon to a chemical reaction. This is an important characteristic showing potentiality of the material application in the photocatalytic process. It can be shown that for a relatively small mass and first order process kinetics, γ is proportional to the reaction rate constant R normalized on the photocatalyst mass (Cheng et al. 2018; Bouslama et al. 2012). This normalized rate reflects

Table 2 Area, average pore radius and pore volume of samples with different titania content (TiC1, TiC2, TiC3, TiC4) and Aeroxide P25 TiO_2

Sample	Specific surface area, m^2/g	Average pore diameter, Å	Pore volume, cm^3/g
MCC	2.5	21	0.004
TiC1	10.2	< 16	0.018
TiC3	27.4	17.7	0.037
TiC4	55.0	19.5	0.060
Aeroxide P25 TiO_2	50.9	16	0.12

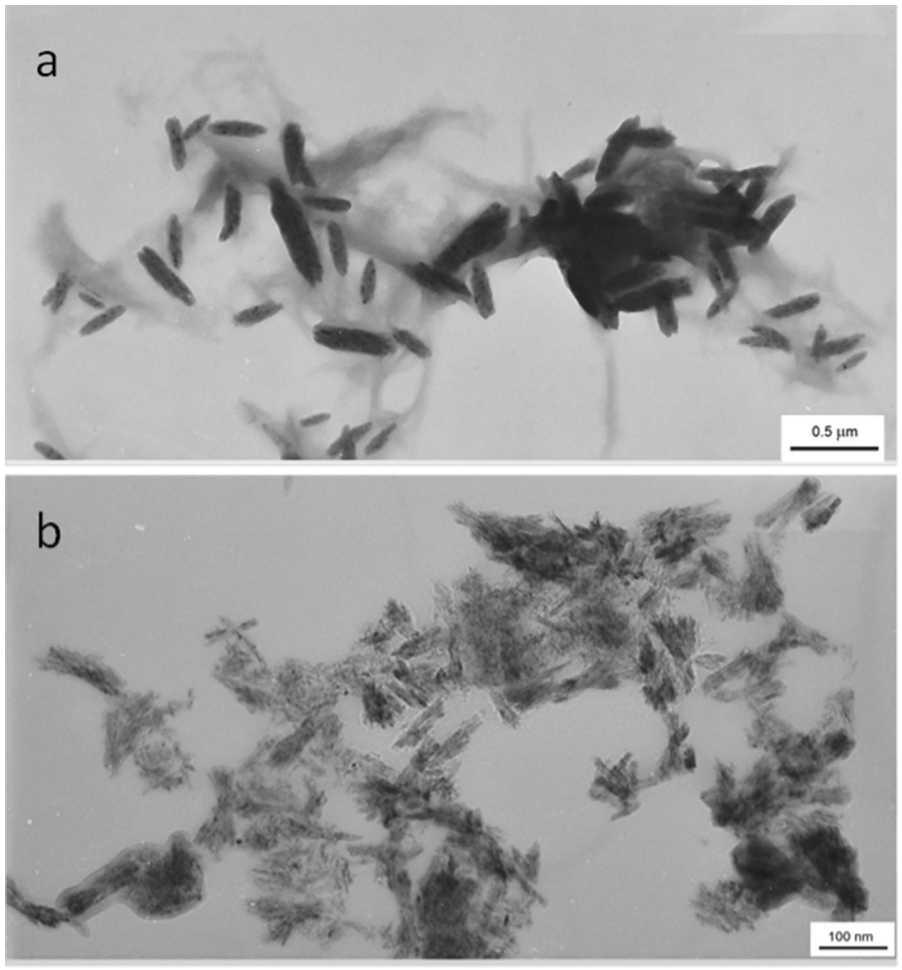

Fig. 8 N_2 adsorption/desorption isotherms for MCC (**a**), TiC1 (**b**), TiC2 (**c**), and TiC4 (**d**)

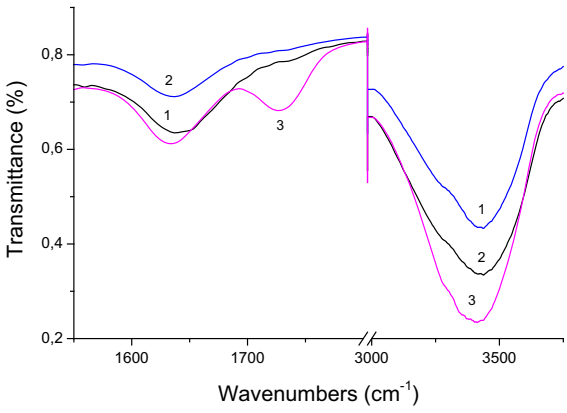

Fig. 9 IR spectra of MCC (1), TiD1 (2) and TiC4 (3) samples

the material effectiveness when the photocatalyst mass is relatively small and decreases at the larger masses due to the saturation of light absorbance in accordance with the Beer-Lambert law. Our first order kinetics permits this comparison of the material activities. Figure 11 shows reaction rates and normalized reaction rates of the best composite materials of TiC series in comparison with the reference TiO_2 P25. These rates, reported in Table 1, were obtained from the slopes of the experimental data presented in semi-logarithmic frame of $\ln(C_0/C)$ versus time of UVA illumination. As expected, the decomposition rate increases with an increase of the photocatalyst mass in both TC and TiO_2 P25 materials because of an increased light absorbance, and saturates when UVA lamp power is totally absorbed by the material. The saturation rates of both types of materials were found similar. Similarly, both TC and TiO_2 P25 materials reached the maximal normalized rates (on

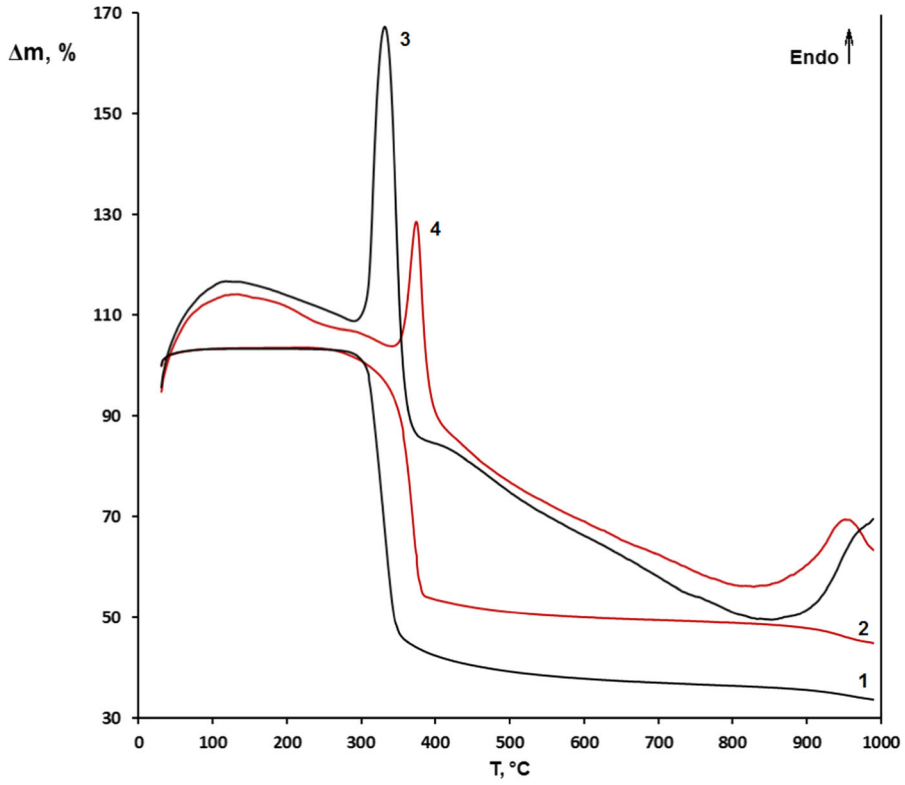

Fig. 10 TG (1, 2) and DSC (3, 4) analyses of MCC (1, 3) and TiC4 (2, 4) samples under argon atmosphere

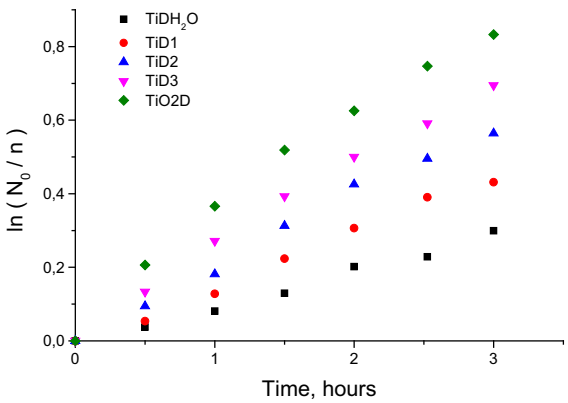

Fig. 11 Kinetics of formic acid decomposition under UV irradiation in aqueous solutions using TiC1, TiC2, TiC3, TiC4, TiC5, TiC6, TiO_2C3 and TiO_2 P25 photocatalysts

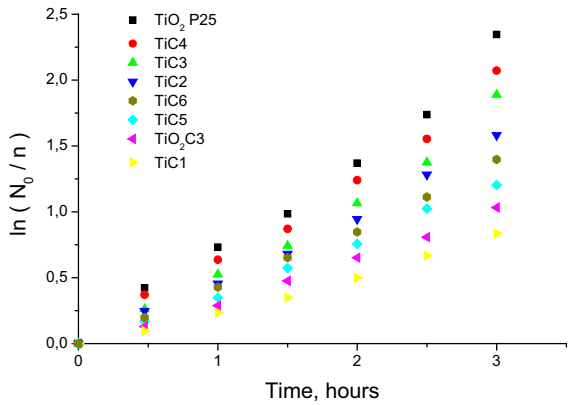

Fig. 12 Absolute (□, △) and normalized on photocatalyst mass (■, ▲) decomposition rates of formic acid observed with TiC (□, ■) and TiO_2 P25 (△, ▲) photocatalysts

photocatalyst mass) at the same TiO_2 loadings, apparently indicating similar effectiveness in screening the UVA lamp photons related to the morphology factors (specific surface area and particle size of titania component). However, values of the maximum normalized rates were different and that of TC photocatalysts was almost two times higher compared to TiO_2 P25. The higher intrinsic efficiency (γ) of TC composites could not be an explanation, since absolute rates at infinite photocatalyst mass of TC and reference materials were similar (Fig. 12). In contrast, finer granulometry of TC composite particles could be a

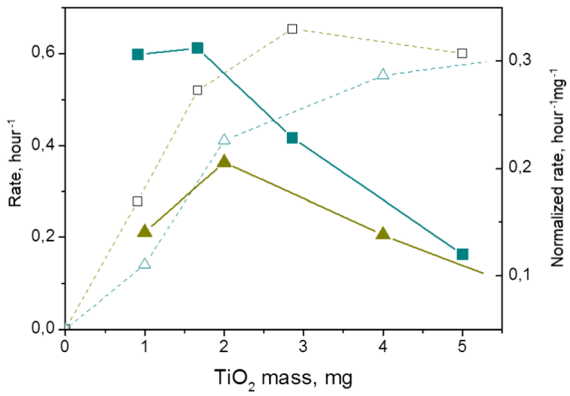

Fig. 13 Kinetics of formic acid decomposition under UV irradiation in aqueous solutions using $TiDH_2O$, TiD1, TiD2, TiD3 and TiO_2D photocatalysts

reason. Indeed large agglomerates of TiO_2 P25 particles (practically of size above 100 nm) possess a significant screened volume, not accessible by UV lamp photons; as a result, this material has a significant mass, which is excluded from the photocatalytic process. In contrast, the TC component, which strongly scatter and not absorbed UVA light (Lu et al. 2013), effectively increase the residence time of UVA photons in the reaction volume; the longer interaction time creates conditions for a more efficient light energy deposition into the photocatalyst.

Conclusion

In this work, novel cellulose-TiO_2 composite photocatalysts were synthetized via solvothermal method in order to assemble microcrystalline organic cellulose and inorganic titania components. Two series of materials were prepared in n-decane and caproic acid solvents. In n-decane, the synthesis resulted in a poor crystallization of anatase titania and the subsequent thermal post treatment destroyed the composites. In contrast, in caproic acid, acting as solvent and reagent, anatase TiO_2 nanoparticles were formed onto the crystalline domains of cellulose. Strong covalent bonds between the organic and inorganic components of the composite were evidenced by IR spectroscopy, ^{1}H NMR and TG/DSC methods. The photocatalytic activity of the synthetized materials was evaluated by the decomposition of formic acid in aqueous solutions under UVA lamp illumination and compared with that of reference photocatalyst Aeroxide P25 TiO_2. The absolute activities of composites and reference photocatalyst were similar. On the other hand, much smaller titania mass was required in order to reach the maximum activity in the prepared composites compared to the reference photocatalyst. This effect was attributed to the organic component, which effectively scatters UVA lamp photons, thus increasing efficiency of the light energy deposition into the inorganic anatase TiO_2 component.

Acknowledgments Authors are grateful to Ministry of Science and Higher Education of Russian Federation for financial support (Project No. 0097-2019-0017).

References

Bouslama M, Amamra MC, Jia Z, Ben Amar M, Brinza O, Chhor K, Abderrabba M, Vignes JL, Kanaev A (2012) Nanoparticulate TiO_2–Al_2O_3 photocatalytic media: effect of particle size and polymorphism on photocatalytic activity. ACS Catal 2:1884–1892. https://doi.org/10.1021/cs300033y

Brandes R, Souza L, Vargas V, Oliveira E, Mikowski A, Carminatti C, Al-Qureshi H, Recouvreux D (2016) Preparation and characterization of bacterial cellulose/TiO_2 hydrogel nanocomposite. J Nano Res 43:73–80. https://doi.org/10.4028/www.scientific.net/JNanoR.43.73

Butman MF, Ovchinnikov NL, Karasev NS, Kochkina NE, Agafonov AV, Vinogradov AV (2018) Photocatalytic and adsorption properties of TiO_2-pillared montorillonite obtain by hydrothermally activated intercalation of titanium polyhydroxo complexes. Beilstein J Nanotechnol 9:364–378. https://doi.org/10.3762/bjnano.9.36

Cardoso GV, Mello LR, Zanatta P, Cava S, Raubach CW, Moreira ML (2018) Physico-chemical description of titanium dioxide–cellulose nanocomposite formation by microwave radiation with high thermal stability. Cellulose 25:2331–2341. https://doi.org/10.1007/s10570-018-1734-2

Cheng K, Chhor K, Passarello JP, Colbeau-Justin C, Kanaev A (2018) Photocatalytic nanoparticulate $Zr_xTi_{1-x}O_2$ coatings with controlled homogeneity of elemental composition. Chem Sel 3:11118–11126. https://doi.org/10.1002/slct.201801732

Dette C, Pérez-Osorio MA, Kley CS, Punke P, Patrick CE, Jacobson P, Guistino F, Jung SJ, Kern K (2014) TiO_2 anatase with a bandgap in the visible region. Nano Lett 12:6533–6538. https://doi.org/10.1021/nl503131s

Farag S, Amr A, El-Shafei A, Ibrahim HM, Asker MS (2017) Influence of bacterial cellulose for synthesis and application of titanium dioxide nanoparticles compared with sol-gel method. In: Proceedings of 60th the IRES international conference, Munich, Germany, pp 15–23

Filippo E, Carlucci C, Capodilupo AL, Perulli P, Conciauro F, Corrente GA, Gigli G, Ciccarella G (2015) Enhanced

photocatalytic activity of pure anatase TiO_2 and Pt-TiO_2 nanoparticles synthesized by green microwave assistant route. Mater Res 18:473. https://doi.org/10.1590/1516-1439.301914

French AD (2014) Idealized powder diffraction patterns for cellulose polymorphs. Cellulose 21:885–896. https://doi.org/10.1007/s10570-013-0030-4

Galkina OL, Sycheva A, Blagodatskiy A, Kaptay G, Katanaev VL, Seisenbaeva GA, Kessler VG, Agafonov AV (2014) The sol-gel synthesis of cotton/TiO_2 composites and their antibacterial properties. Surf Coat Technol 253:171–179. https://doi.org/10.1016/j.surfcoat.2014.05.033

Garusinghe UM, Raghuwanshi VS, Batchelor W, Garnier G (2018) Water resistant cellulose-titanium dioxide composites for photocatalysis. Sci Rep 8:2306. https://doi.org/10.1038/s41598-018-20569-w

Gorbovyi P, Uklein A, Tieng S, Traore M, Chhor K, Museur L, Kanaev A (2011) Novel nanostructured pHEMA-(oxo)TiO_2 hybrid materials with efficient light-induced charge separation. Nanoscale 3:1807–1812. https://doi.org/10.1364/OME.3.000533

Habibi S, Jamshidi M (2020) Synthesis of TiO_2 nanoparticles coated on cellulose nanofibers with different morphologies: Effect of the template and sol-gel parameters. Mater Sci Semicond Process 109:104927. https://doi.org/10.1016/j.mssp.2020.104927

He D, Li Y, Wang J, An Q (2016) Tunable nanostructure of TiO_2 reduced oxide composite for high photocatalysis. Appl Microsc 46:37–44. https://doi.org/10.9729/AM.2016.46.1.37

Ioelovich M (2014) Cellulose: nanostructured natural polymer. Lap Lamber Acad, Saarbrucken, p 100

Kaseem M, Hamad K, Rehman ZU (2019) Review of recent advances in polylactic acid/TiO_2 composites. Materials 12:3659. https://doi.org/10.3390/ma12223659

Kayaalp M, Rathousk J, Bein T (2014) Tailoring the morphology of mesoporous titania thin film through biotemplating with nanocrystalline cellulose. J Am Chem Soc 136:5930–5937. https://doi.org/10.1021/ja411292u

Khalid A, Ullah H, Ul-Islam M, Khan R, Khan S, Ahmad F, Khal T, Wahid F (2017) Bacterial cellulose–TiO_2 nanocomposites promote healing and tissue regeneration in burn mice model. RSC Adv 7:47662–47668. https://doi.org/10.1039/c7ra06699f

Kuznetsov AI, Kameneva O, Bityurin N, Rozes L, Sanchez C, Kanaev A (2009) Light-induced photopattering of organic-inorganic TiO_2 based hybrid materials with tunable interfacial electron transfer. Phys Chem Chem Phys 11:1248–1257. https://doi.org/10.1039/B814494J

Li Y, Zhang JC, Kong F, Li W, Yang C, Hsiao BS (2020) Facile synthesis of TiO_2/CNC nanocomposites for enhanced Cr(VI) photoreduction: synergistic roles of cellulose nanocrystals. Carbohydr Polym 233:115838. https://doi.org/10.1016/j.carbpol.2020.115838

Lu Y, Sun Q, Liu T, Yang D, Liu Y, Li J (2013) Fabrication, characterization and photocatalytic properties of millimeter-long TiO_2 fiber with nanostructures using cellulose fiber as a template. J Alloys Compd 577:569–574. https://doi.org/10.1016/j.jallcom.2013.06.183

Luo Y, Xu J, Huang J (2014) Hierarchical nanofibrous anatase-titania–cellulose composite and its photocatalytic property. CrystEngComm. https://doi.org/10.1039/c3ce41906a

Melvin NHK, Leo CP (2019) The coherence between TiO_2 nanoparticles and microfibrillated cellulose in thin film for enhanced dispersal and photodegradation of dye. Prog Org Coat 132:70–75. https://doi.org/10.1016/j.porgcoat.2019.02.017

Morawski AW, Kusiak-Nejman E, Przepiórski J, Kordala R, Pernak J (2013) Cellulose-TiO_2 nanocomposite with enhanced UV–Vis light absorption. Cellulose 20:1293–1300. https://doi.org/10.1007/s10570-013-9906-6

Morshed MN, Azad SA, Deb H, Shaun BB, Shen XL (2020) Titania-loaded cellulose-based functional hybrid nanomaterial for photocatalytic degradation of toxic aromatic dye in water. J Water Process Eng 33:101062. https://doi.org/10.1016/j.jwpe.2019.101062

Mory K (2005) Photo-functionalized materials using g nanoparticles: photocatalysis. KONA Powder J 23:205–214. https://doi.org/10.14356/kona.2005023

Oliveira AC, Santos MS, Brandão LMS, Resende ITF, Leo IM, Morillo ES, Yerga RMN, Fierro JLG, Egues SMS, Figueiredo RT (2017) The effect of cellulose loading on the photoactivity of cellulose-TiO_2 hybrids for hydrogen production under simulated sunlight. Int J Hydrog Energy 42:28747–28754. https://doi.org/10.1016/j.ijhydene.2017.09.022

Postnova I, Kozlova E, Cherepanova S, Tsybulya S, Rempel A, Shchipunov Y (2015) Titania synthesized thorough regulated mineralization of cellulose and its photocatalytic activity. RSC Adv 5:8544–8551. https://doi.org/10.1039/C4RA15862H

Rahmawati F, Fadillah M, Mudjijono I (2017) Composite of nano-TiO_2 with cellulose acetate membrane from nata de coco (Nano-TiO_2/CA(NDC)) for methyl orange degradation. J Mater Environ Sci 8:287–297

Sathasivam S, Bhachu SD, Li Y, Chadwick N, Althabaiti SA, Alyobi AO, Basahel SN, Carmalt CJ, Parkin IP (2015) Tungsten doped TiO_2 with enhanced photocatalytic and opt-electrical properties via aerosol assisted chemical vapor deposition. Sci Rep 4:10952–10956. https://doi.org/10.1038/srep10952

Segal L, Creely JJ, Martin AE, Contrad CM (1959) An empirical method for estimating the degree of crystallinity of native cellulose using the X-ray diffractometer. Text Res J 29(10):786–794. https://doi.org/10.1177/004051755902901003

Shahrezaei M, Habibzadeh S, Babaluo AA, Hosseinkhni H, Haghighi M, Hasanzedah A, Tahmasebpour R (2017) Study of synthesis parameters and photocatalytic activity of TiO_2 nanostructures. J Exp Nanosci 12:45. https://doi.org/10.1080/17458080.2016.1258495

Sharon M, Modi F, Sharon M (2016) Titania based nanocomposite as a photocatalyst: a review. AIMS Mater Sci 3:1236–1254. https://doi.org/10.3934/matersci.2016.3.1236

Shevtsova TA, Zlotski SV (2018) Facile sol-gel synthesis of metal oxide nanoparticles in a cellulose paper template. Doklady Bguir 112:113–115

Sirvio JA, Visanko M, Heiskanen JP, Liimatainen H (2016) UV-absorbing cellulose nanocrystals as functional reinforcing fillers in polymer nanocomposite films. J Mater Chem A 4:6368–6375. https://doi.org/10.1039/C6TA00900J

Sun D, Yang J, Wang X (2010) Bacterial cellulose/TiO_2 hybrid nanofibers prepared by the surface hydrolysis method with molecular precision. Nanoscale 2:287–292. https://doi.org/10.1039/b9nr00158a

Tang B, Chen H, Peng H, Wang Z, Huang W (2018) Graphene modified TiO_2 composite photocatalysts: mechanism. Progress Perspect Nanomater 8:105. https://doi.org/10.3390/nano8020105

Tieng S, Kanaev A, Chhor K (2011) New homogeneously doped Fe(III)–TiO_2 photocatalyst for gaseous pollutant degradation. Appl Catal A 399:191–197. https://doi.org/10.1016/j.apcata.2011.03.056

Wang SB, Pan L, Song JJ, Mi W, Zou JJ, Wang L, Zhang X (2015) Titanium-defected undoped anatase TiO_2 with p-type conductivity, room-temperature ferromagnetism, and remarkable photocatalytic performance. J Am Chem Soc 137:2975–2983. https://doi.org/10.1021/ja512047k

Wang W, Wang J, Shi X, Yu Z, Song Z, Dong L, Jiang G, Han S (2016) Synthesis of Mesoporous TiO_2 Induced by NanoCellulose and Its Photocatalytic Properties. BioResources 11:3084–3093. https://doi.org/10.15376/biores.11.2.3084-3093

Wittmar A, Thierfeld H, Köcher S, Ulbricht M (2015) Routes towards catalytically active TiO_2 doped porous cellulose. RSC Adv 5:35866–35873. https://doi.org/10.1039/C5RA03707G

Xiao H, Li J, He B (2017) Anatase-titania templated by nanofibrillated cellulose and photocatalytic degradation for methyl orange. J Inorg Organomet Polym Mater 27:1022–1027. https://doi.org/10.1007/s10904-017-0550-8

Yatsenko DA, Medvedeva TB (2019) Estimating crystality index of microcrystalline cellulose using diffraction methods. J Struct Chem 60:1430–1436. https://doi.org/10.1134/S0022476619090075

Zdravkov A, Kudryashova J, Kanaev A, Povolotskiy A, Volkova A, Golikova E, Khimich N (2015) A new solvothermal route to efficient titania photocatalyst. Mater Chem Phys 160:73–79. https://doi.org/10.1016/j.matchemphys.2015.04.008

Zhang X, Chen YL, Liu RS, Tsai DP (2013) Plasmonic photocatalysis. Rep Prog Phys 76:046401. https://doi.org/10.1088/0034-4885/76/4/046401

Zlotski SV, Uglov VV (2017) Facile sol-gel synthesis of metaloxide nanoparticles in a cellulose paper template. J Nanomed Nanotechnol S8:002. https://doi.org/10.4172/2157-7439.S8-002

Publisher's Note Springer Nature remains neutral with regard to jurisdictional claims in published maps and institutional affiliations.